# 2D/3D NEGF modeling of the impact of random dopants /dopant aggregation in silicon nano-transistors

John R. Barker
Department of Electronics and Electrical Engineering,
University of Glasgow
Glasgow G12 8LT, United Kingdom
jbarker@elec.gla.ac.uk

***Abstract*— The discrete nature of dopants becomes apparent in nano-scaled devices leading to microvariability problems which cause large fluctuations in the performance of macroscopically identical devices. Since self-averaging fails, the approach reviewed here utilises self-consistent non-equilibrium Green function modelling to evaluate the effects of discrete random dopants in source and drain non-perturbatively.**

***Keywords-component; random dopants, nanotransistors, Green functions, impurities, resonances, resonant tunnelling.***

## I. INTRODUCTION

Silicon nano-transistors have been demonstrated with 5 nm channel lengths [1]. But a major issue confronting the extension of the road map is the micro-variability problem: devices which are fabricated to the same *macroscopic* specification (doping densities, feature sizes and scales, edge and interface definition) will have different device characteristics (threshold voltage, channel conductance, current drive) because the discrete nature of the dopants and the random variability in edge/interface definition means that each device is *microscopically* different. This causes large differences between the performances of individual devices. New device architectures may help; and here we focus on two classes of MOSFET: the double gate device (Fig. 1a) and the wrap-round gate nanowire device (Fig. 1b). Although the impact of discrete dopants in the device channel has been studied extensively less attention has been focussed on the granularity of the source-drain regions. An elegant experimental study [2] has shown directly that the source-drain extensions in quite large conventional MOSFETs show charge granularity. This work inspired a first attempt to understand the issues using a self-consistent 2D Green function simulation of double gate devices [3]. The results are summarised in section III. However, once it is necessary to treat dopants as discrete it becomes crucial to study the problem in three dimensions especially as quantum confinement becomes important. For this purpose we have developed a fully self-consistent non-equilibrium Green function (NEGF) simulator [4] for treating the problem non-perturbatively (section II). Self-consistancy, imposed by coupling the transport equations to Poisson's equation ensures a correct treatment of charge conservation and screening.

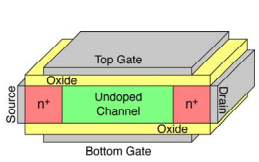


Figure 1 (a) Double Gate Device

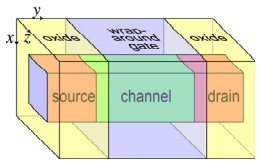


Figure 1 (b) Wrap-round gate device

For *n*-channel devices the source/drain doping involves attractive Coulomb centres (ionized donors) which within the quantum transport theory of nanowires give quite different effects to repulsive Coulomb centres associated with acceptors (section IV). The attractive potentials create quasi-bound electronic states which lead to both zeros and resonances in the energy-resolved transmission function. Both Breit-Wigner and Fano resonances occur as anticipated in simplified model studies [5-10]. These effects are highly sensitive to the shape of the self-consistent impurity potentials and to the proximity to boundaries. Only now have we been able to achieve stable convergent solutions to the 3D NEGF simulator for narrow channel n-channel devices with localised donors [11]. These effects underpin the influence of discrete donors in source and drain on threshold voltage and current behaviour (section V).

## II. GREEN FUNCTION METHODOLOGY

The Green function methodology is defined in detail elsewhere [3, 4] . An appropriate effective-mass Hamiltonian is used to define the energy-resolved retarded Green function $G^R(\mathbf{r},\mathbf{r}';E)$ and corresponding advanced Green function $G^A$ that describe the steady-state quantum kinetics. These are used to compute the less-than Green function $G^<(\mathbf{r},\mathbf{r}';E)$. The energy-resolved charge density and current density follow:

$$n(\mathbf{r},E) = (-i/2\pi)G^<(\mathbf{r},\mathbf{r};E) \quad (1)$$

$$\mathbf{J}(\mathbf{r},E) = (-\frac{ie\hbar}{2}\mathbf{m}^{-1}*)\bullet[\nabla - \nabla']G^<(\mathbf{r},\mathbf{r}',E)\big|_{r'=r} \quad (2)$$

For a single-body pure quantum state of energy $E$ described by an extended wave function $\psi(\mathbf{r};E)$ the function $G^{<}(\mathbf{r},\mathbf{r}';E)$ corresponds to the correlation function:

$$g(\mathbf{r},\mathbf{r}';E)=\psi^{*}(\mathbf{r};E)\psi(\mathbf{r}';E) \quad (3)$$

The thermally averaged Green functions determine the charge density which is used to compute the electrostatic potential using Poisson's equation. The electrostatic potential is fed back into the effective Hamiltonian so that the impurity potential is self-consistently screened. The iterative cycle is continued until convergence is achieved (typically 25 interations). A set of sophisticated recursive algorithms reduce the complexity of the problem and implement the contact boundary conditions [4, 6, 12].

## III. 2D MODEL FOR SOURCE AND DRAIN DOPING

We have previously studied the effect of deviations from doping uniformity in source and drain on the performance of sub 20 nm silicon double-gate MOSFET devices [3]. The model assumed a continuous charge distribution with randomly located regions of high doping: the aggregation model. Individual dopants were not resolved. Incoherent impurity scattering in the source and drain regions was neglected. The current-voltage characteristics $I_D$-$V_G$ were computed for devices that differed only in the microscopic arrangement of the randomly distributed high doping regions. We also studied devices that differed in the *number* of these clusters. An ensemble of devices with fluctuating numbers of clusters was constructed based on a Gaussian distribution centered on the mean cluster number derived from the average doping concentration in the source/drain. An average lateral symmetry was assumed for the double gate MOSFET. Therefore, only inhomogeneities in the doping in the plane of the simulation were considered. The devices studied had 12 nm channel lengths. Fig. 2 shows a typical dopant aggregation distribution with the corresponding electrostatic potential and electron density computed from the self-consistent 2D method. The computed current-voltage characteristics (Figs. 3-4) are monotonic and they are most strongly affected by the fluctuations in the total number of high doping regions (Fig. 4). Threshold voltages shifts around 100 mV and on-current fluctuations around 50 percent are obtained from the simulations. However, the sub-threshold slope is almost independent of the microscopic cluster distribution.

## IV. 3D SCATTERING ON ATTRACTIVE POTENTIALS

In the absence of impurities the energy-resolved conductance of a hard walled straight nanowire is a stepped function of energy, each step corresponding to the onset of a new conducting channel associated with the lateral sub-band structure. For negatively charged impurities these steps are smeared out to an extent that depends on the numbers of impurities. In rare cases, two negatively charged impurities may be closely in line with the channel such that a quasi-bound state exists between the two. This rare case is a special example of a much more common situation that arises with positively charged impurities in gated devices as we explore later.

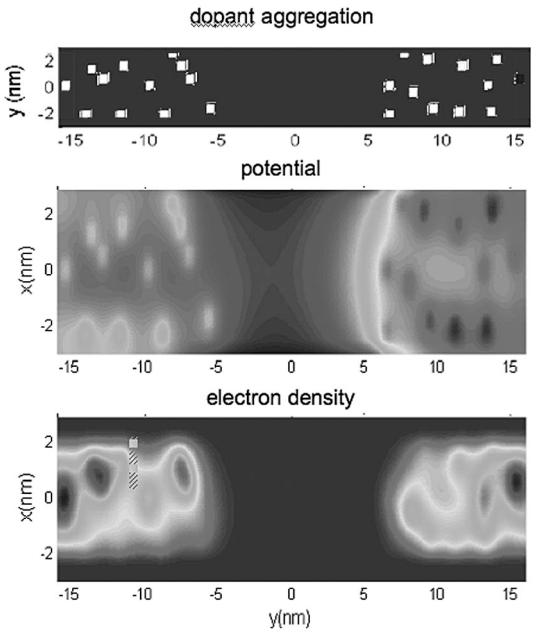


Figure 2: 2D NEGF study of Double Gate Device (12 nm channel) Showing dopant aggregation clusters, electrostatic potential and electron density

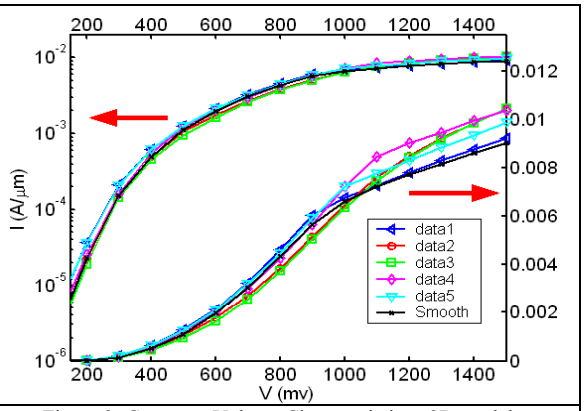


Figure 3: Current – Voltage Characteristics : 2D model spatial disorder

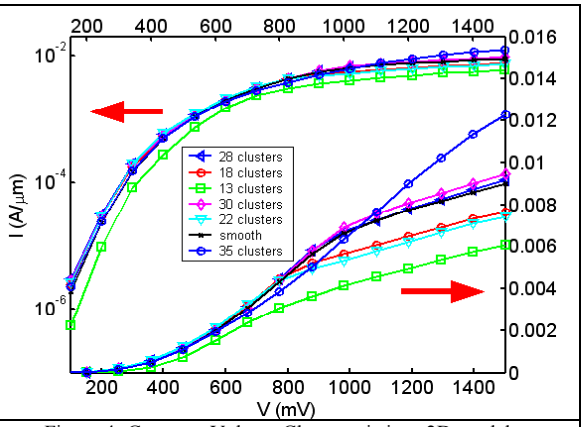


Figure 4: Current - Voltage Characteristics : 2D model number fluctuations

Single positively charged impurities provide a wealth of features in quantum transport [5-10]. The energy-resolved conductance may exhibit a dip preceding each conductance step (except the first step). The dips are due to back-scattering by a quasi-bound state originating from an evanescent mode in the next sub-band. This is a multi-mode effect. Early studies of this effect [10] used delta function models requiring over 100 modes to obtain convergent results. The general interaction between a discrete state in the continuum and the continuum leads to a quasi-bound state and a characteristic resonant line shape in the transmission or energy –resolved conductance: the Fano effect. The form of the Fano resonance is complicated by the parameters of the originating attractive potential and the effects of size confinement. Simple models have been invoked to explain Fano resonance phenomena in nanowires but without using Coulomb potentials or indeed electrostatically self-consistent potentials or taking into account realistic device geometries. All the resonance phenomena previously reported from non-self consistent simplified models are found to occur in our self-consistent NEGF studies of discrete dopants ([11, 14] and to be reported in detail elsewhere).

Following [11] in Fig. 5 we give a schematic of the self-consistent potential for a single attractive Coulomb impurity in the centre of a wrap-round gate nanowire transistor (2.2 nm X 2.2 nm X 14 nm; 10 nm channel) below threshold. The source and drain are considered to be continuously doped in this case with a doping concentration of $10^{20}$cm$^{-3}$. Here, in the absence of the impurity the potential profile along the channel is the normal barrier potential. Adding the attractive Coulomb potential burns a hole in this profile to produce the sombrero shape. In the absence of size confinement this self-consistent potential has discrete bound states and a continuum set of states with an embedded quasi-bound state. The latter is a resonant tunnelling state. This state aids the screening of the impurity by allowing charge to accumulate in the effective quantum well. The geometry of the device is crucial. The lateral size quantization induces sub-band structure which picks up the resonant levels in different modes leading to complex Fano structures. The principal effect of the resonant tunnelling level is to induce a strong resonant peak following the onset of each sub-band transmission step as shown in Fig. 6. The plateau structure is lost because of reflection (scattering) from the impurity except at the resonance where unit transmission ensues. Thus the net conductance is substantially reduced. In Fig. 7 we compare the off-current behaviour for the impurity free channel with that having a single attractive Coulomb impurity at the channel centre. The off-current is significantly increased by the impurity, partly due to reduction of the gate barrier and partly to the introduction of the resonant tunnelling channel. By turning on the gate potential the sombrero shaped potential may be tuned in shape and strength to alter the transmission profiles. Moving the impurity towards the boundaries reduces the effect.

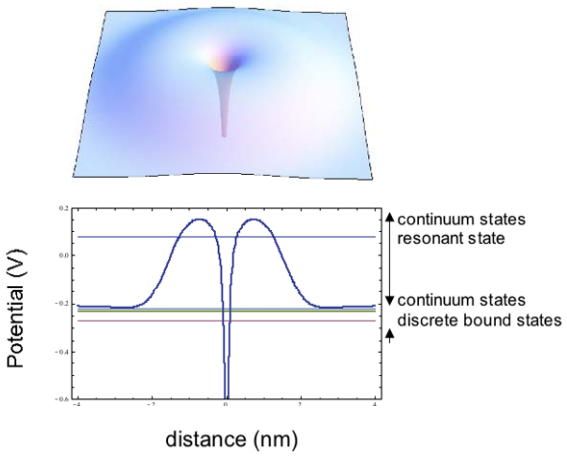


Figure 5: Self-consistent potential in channel: schematic

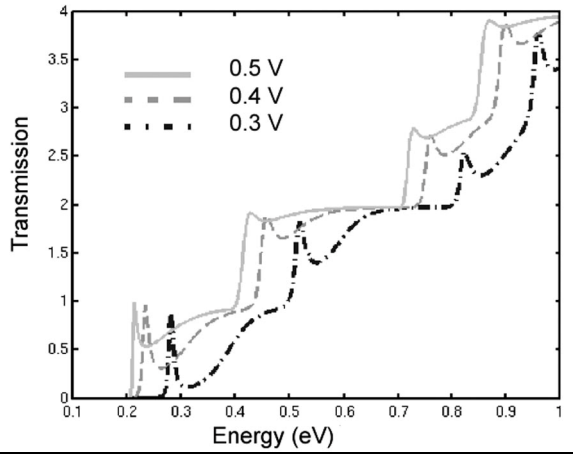


Figure 6: Transmission as a function of energy for wrap-round nanowire device with a single attractive Coulomb centre in middle of channel at different gate voltages. Channel length 10 nm. Source/Drain doping continuously doped at $10^{20}$ cm$^{-3}$.

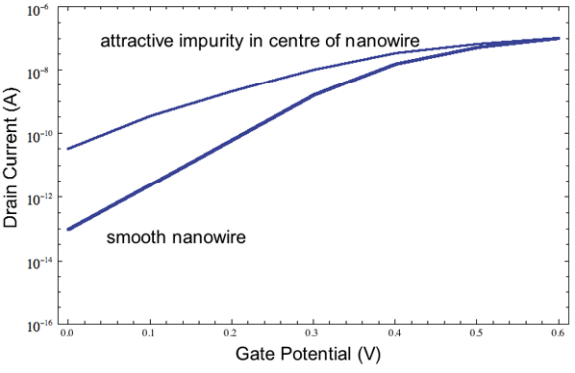


Figure 7: Off – Current versus gate voltage characteristics with and without attractive impurity

## V. 3D MODEL OF SOURCE AND DRAIN DOPANTS

Let us now consider a 3D wrap-round gate device with *atomically* resolved source and drain [14].

Devices with 2.2 nm X 2.2 nm cross section with un-doped channels with lengths 4 nm to 6 nm were studied. The source and drain extensions are each resolved *atomically* over regions of length 4 nm beyond which the doping is treated as continuous (a good approximation within mean field theory).

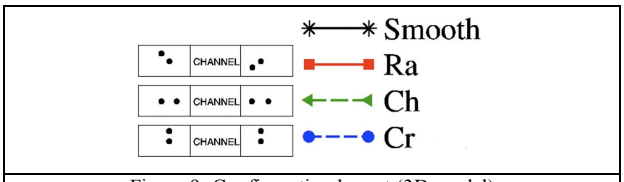


Figure 9: Configuration layout (3D model)

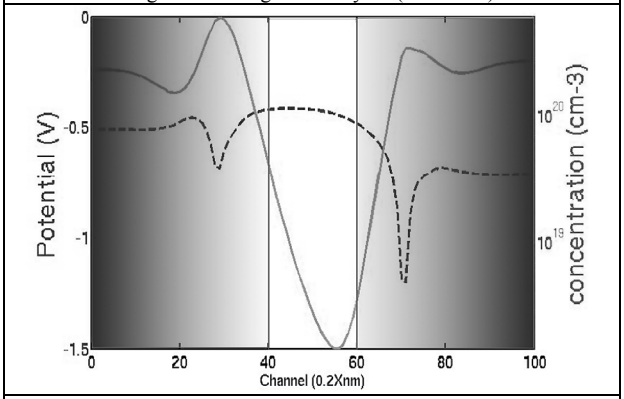


Figure 10: Electron density (full line) and Potential (dashed line) Shading shows transition to continuum doping.

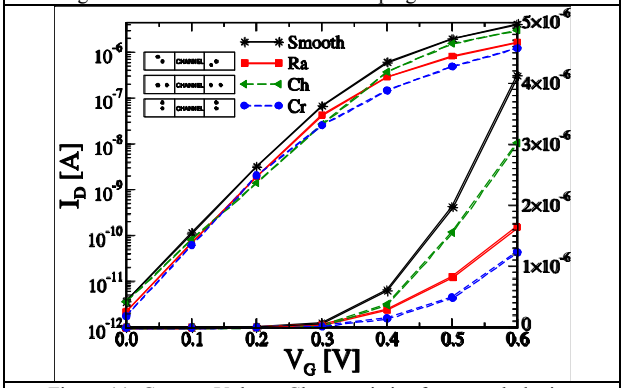


Figure 11: Current-Voltage Characteristics for smooth doping model versus 3 discrete dopant configurations (3D model) [14]

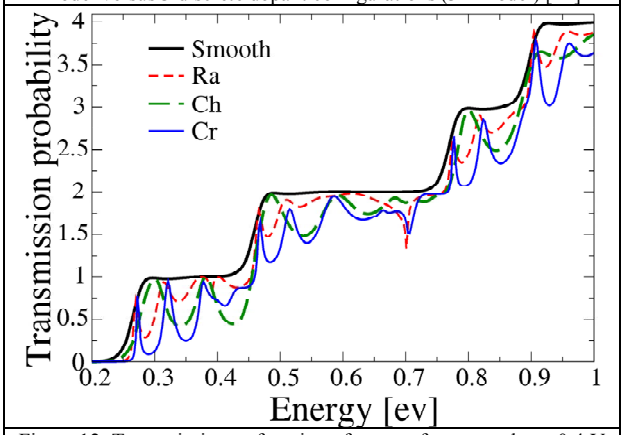


Figure 12: Transmission as function of energy for gate voltage 0.4 V For continuous doping and discrete dopant variants of source and drain doping (3D model) [ 14]

The doping is set at $10^{20}$cm$^{-3}$ leading to just two dopants in each of the source and drain extensions. The configurations for 4 devices are shown in Fig. 9. The effective masses of the valleys are extracted from Tight Binding calculations [13]. Fig. 10 shows the potential profile and electron density in a cross section through the middle of the device for case *Ra*. The results follow the pattern discussed in IV: the potential around each dopant has a deformed sombrero structure. The barrier lowering and resonant tunnelling allow charge to accumulate near the impurity and help screen the bare Coulomb potential. Fig. 11 shows a set of current-voltage characteristics on linear and log scales for the four configurations[14]. The average threshold voltage shift is 20 mV. The sub-threshold slope becomes worse for the case of the impurities aligned in the middle of the wire. In general, the sub-threshold slope changes as a function of the particular impurity configuration. The effect of the discreteness of the impurities on the on-current is more dramatic. The on-current in the *Cr* case is *30%* of the corresponding value for the smooth case, whereas for the *Ch* case the current is *73%* of the smooth device.

The current-voltage characteristics may be understood from the transmission curves for the different configurations. Fig. 12 gives the results for $V_G$ = 0.4 V. The resonant structure is complicated, but as before, the electrons are partially reflected due to the impurity potential, decreasing the total transmission except at resonance. At low gate bias, this effect is less noticeable due to the gate barrier and quite similar to the smooth one. The transmission in the smooth device is higher than in the *Ch* device for the energy intervals (0.5,0.55) and (0.6,1.0) eV, but in the interval (0.55,0.6) eV the transmission in the *Ch* device is higher than in the smooth one (the Fermi energy at source is 0.19 eV*)*., produces similar values for both devices.The backscattering increases with gate bias yielding a low transmission except around the resonance energies. It follows that at high gate biases, the difference between the currents of the smooth device and the other devices increases. At $V_G \geq$ 0.4 V the transmission for the *Ch* case becomes larger than for the *Ra* and *Cr* cases in the interval (0.0,0.3) eV except around the resonance peak. Since the Fermi level in the source is ~ 0.2eV, we expect more current in the *Ch* case than in the other two cases.

## REFERENCES


[1] T-Y Liow et al, VLSI Tech. Symp. 38 (2008).

[2] H.Fukotome, Y. Momiyama, E. Yoshida, M. Okuno, T.Itakura and T. Aoyama, IEDM Technical Digest (2005).

[3] A. Martinez, J. R. Barker, A. Svizhenko, M. P. Anantram, and A. Asenov, IEEE Trans. Nanotech.:**6**, 438 (2007).

[4] A. Martinez, M. Bescond, J.R. Barker, A. Svizhenko, M. P. Anatram, C. Millar and A. Asenov, IEEE Trans. Elec. Dev. **54**, 2213 (2007).

[5] R. C. Bowen, W. R. Frensley, G. Klimeck and R. K. Lake, Phys.Rev. **B 52**, 2754 (1995).

[6] R. Lake, G. Klimeck, R. C. Bowen, and D. Jovanovich, J. Appl. Phys. **81**, 7845 (1997).

[7] J.H. Bardarson, I. Magnusdottir, G. Gudmundsdottir, C.S. Tang, A. Manolescu and V. Gudmundsson, Phys.Rev. **B 70**, 245308 (2004).

[8] V. Vargiamidis and H. M. Polatogluo, Phys.Rev. **B 72**, 195333 (2005).

[9] P. F. Bagwell, Phys. Rev. B **41**, 10 354 (1990).

[10] C.S. Kim *et al*, Phys.Rev. **B 60**, 10962 (1999)

[11] A. Martinez, J.R. Barker, A.R. Brown, A. Asenov and N. Seoane, these proceedings, SISPAD (2008).

[12] A.Svizhenko, M.P. Anatram, T.R. Govindan, B. Siegel, R. Venugopal, J.Appl. Phys. **91**, 2343 (2002).

[13] K. Nehari, N. Cavassilas, J. L. Autan, M. Bescond, D. Munteau and M. Lanoo, Solid State Electronics, 5**0**, 716 (2006).

[14] N. Seoane, A. Martinez, A. R. Brown, J. R. Barker and A. Asenov, Silicon Nanoelectronics Workshop, Honolulu, HI, USA (2008).